## References

[1]Pankhurst, R. C., and Holder, D. W., "Wind-Tunnel Technique," Pitman & Sons, Ltd., London, 1952.

[2]Rae, W. H., Jr., and Pope, A., "Low-Speed Wind Tunnel Testing," Wiley, New York, 1984.

[3]Garner, H. C., Rogers, E. W. E., Acum, W. E. A., and Maskell, E. C., "Subsonic Wind Tunnel Wall Corrections," AGARDograph 109, Oct. 1966.

[4]Hackett, J. E., Sampath, S., and Phillips, C. G., "Determination of Wind Tunnel Constraint Effects by a Unified Wall Pressure Signature Method," NASA CR-166, 186, June 1981.

[5]Ashill, P. R., and Keating, R. F. A., "Calculation of Tunnel Wall Interference from Wall-Pressure Measurements," *Aeronautical Journal*, Vol. 92, No. 911, 1988, pp. 36–52.

[6]Katz, J., "Integration of Computational Methods into Automotive Wind Tunnel Testing," Society of Automotive Engineers Paper 89-0601, Detroit, MI, Feb. 1989.

[7]Browne, L., and Katz, J., "Application of Panel Methods to Wind Tunnel Wall Interference Corrections," AIAA Paper 90-0007, Jan. 1990.

[8]Katz, J., and Walters, R., "Investigation of Wind-Tunnel Wall Effects in High Blockage Testing," AIAA Paper 95-0438, Jan. 1995.

[9]Abbott, I. H., and Von Doenhoff, A. E., "Theory of Wing Sections," Dover, New York, 1959, pp. 578, 579.


# Unstructured Euler Flutter Analysis of Two-Dimensional Wing–Tail Configuration


Dartzi Pan* and Jen-Chieh Cheng†
*National Cheng Kung University, Tainan 70101, Taiwan, Republic of China*


## Introduction

THE unsteady interferences from vortical disturbances in the flow can be important for the aeroelastic behavior of lifting surfaces. Frequently, these interferences alter the flowfield significantly, with consequent changes in aerodynamic loading and aeroelastic behavior of the lifting surfaces. In transonic regime where shock wave strength and position are sensitive to small changes in flow parameters, vortical wakes may be shed from the wing for a variety of flow conditions. The downstream tail is under the direct influence of such vortical wakes and may experience significant changes in aeroelastic characteristics. It is thus of practical importance to investigate the aerodynamic interferences and aeroelastic characteristics of the tail, under the influence of a stationary or oscillating forewing.

Most of the aeroelastic studies in the literature focus on the flutter behavior of an isolated airfoil. There have been few concerns about the aeroelastic characteristics of two-airfoil systems, which are the two-dimensional representation of a canard–wing or wing–tail configuration. Shankar and Malmuth[1] performed the steady transonic small disturbance calculations for the two-dimensional canard–wing systems. Batina[2] studied the aeroelastic stability and flutter of two-dimensional wing–canard configurations in frequency domain. These studies are all based on the transonic small disturbance equations, where the shock is weak and the airfoil motion is assumed small. Recently, the Euler solver on dynamic unstructured meshes are employed for more realistic aeroelastic studies. For example, Rausch et al.[3] performed the Euler flutter analysis of airfoils using unstructured dynamic meshes. Batina[4] calculated the unsteady flow over an aircraft oscillating with a fuselage bending mode. The Euler solvers in these studies are based on multistage Runge–Kutta time-stepping schemes with added artificial dissipation terms to control the stability and the oscillation across solution discontinuities.

Received May 20, 1993; presented as Paper 94-0284 at the AIAA 32nd Aerospace Sciences Meeting and Exhibit, Reno, NV, Jan. 10–13, 1994; revision received Jan. 15, 1995; accepted for publication March 15, 1995. 

*Associate Professor, Institute of Aeronautics and Astronautics. Member AIAA.

†Graduate Student, Institute of Aeronautics and Astronautics.

## Euler Solver on Dynamic Unstructured Mesh

In this study, an upwind unstructured Euler solver based on Roe's approximate Riemann solver[5,6] and a two-degree-of-freedom aeroelastic solver are employed for the time-domain flutter analysis of wing–tail configurations. A dynamic grid method is implemented by treating the mesh as a spring network where each edge of each cell represents a spring with stiffness inversely proportional to the length of that edge. The outer boundary of the mesh is held fixed in space, while the inner boundaries such as the surfaces of the wing and the tail are allowed to move in a prescribed manner or as determined by aeroelastic solver. The positions of the interior nodes are then determined by the static equilibrium of the spring system. The geometrical conservation laws (GCL) are enforced by the procedure proposed by Vinokur,[7] which avoids the explicit integration of the cell volume.

## Time-Marching Aeroelastic Solver

The aeroelastic solver takes the aerodynamic loads computed by the Euler solver as the input forcing functions. It then solves the classical aeroelastic equations of motion for a typical section airfoil in terms of plunge and pitch degree of freedom. Considering the inertia, elastic, and aerodynamic forces, the nondimensional aeroelastic equations of motion without damping can be written as

$$M\ddot{y} + Ky = Gu \tag{1}$$

where $y = [h\alpha]^T$ is the vector of plunge displacement $h$ (positive when downward) and pitch displacement $\alpha$ (positive when nose-up) measured from the assumed static operating condition; $u = [(C_L - C_{L0})(C_M - C_{M0})]^T$ is the vector of aerodynamic loads with the static load $C_{L0}$ and $C_{M0}$ subtracted; and matrices $M$, $K$, and $G$ are the coefficient matrices of generalized mass, stiffness, and forces, respectively. In particular, a speed index $V^* = 2U_\infty/c\omega_\alpha$ is involved in matrix $K$, where $c$ is the chord length and $\omega_\alpha$ is the uncoupled natural frequency in pitching. It is convenient to put Eq. (1) in a linear state equation form:

$$\dot{x} = Ax + Bu \tag{2}$$

where $x = [h\alpha\dot{h}\dot{\alpha}]^T$ and matrices $A$ and $B$ are made of $M$, $K$, and $G$. After approximations for a small time step, Eq. (2) is integrated in time by the algorithm of Edwards et al.[8]:

$$x_{n+1} = \Phi x_n + \Theta B(3u_n - u_{n-1})/2 \tag{3}$$

where $\Phi$ is the state-transition matrix, and $\Theta$ is the integral of $\Phi$ from time step $n$ to $n + 1$. By varying $V^*$, the time history of displacement is recorded and processed by a fast Fourier transform (FFT) analysis or a modal identification technique by Bennert and Desmarais[9] to identify its damping and frequency. The system is said to be fluttering when the system damping is negative.

## Tail Flutter with a Stationary Forewing

A two-airfoil system is used to represent a two-dimensional wing–tail configuration. NACA 0012 airfoil section is chosen for both airfoils. The tail chord is normalized to unit and the wing chord is twice that of the tail chord. The structural parameters of the tail are taken from the much studied configuration designated as case A by Isogai.[10] The flutter boundary of an isolated NACA 0012 and two wing–tail configurations are investigated. For model 1, the horizontal separation $S_t$ between the quarter-chord points of the airfoils is 3.75, the vertical offset $O_t$ between the quarter-chord point of the airfoils is 0, and the angle of attack of both airfoils is 0. This is a symmetric case with no aerodynamic loads at the equilibrium position. For model 2, $S_t$ and $O_t$ are the same as in model 1, but the angle of attack is $-2.5$ deg for the wing and 0 for the tail. Note that since the wing has a negative angle of attack, a downward lift is produced on the wing. The mesh employed contains 9232 triangular cells with 128 nodes on the wing surface and 64 nodes on the tail surface. The far-field boundary is 15 wing chord lengths away.

The freestream has a Mach number $M_\infty = 0.8$ and an angle of attack $\alpha = 0$. With the wing held stationary, a steady-state solution is obtained first and then the tail motion is integrated in time with a prescribed initial disturbance of $\dot{h} = 0.002$. The Euler implicit method is used to integrate the flow solver, and about 3000 time steps are taken to complete one cycle of oscillation. Figure 1 is the result of modal identification. A linear interpolation between the calculated dampings indicates that the flutter speed for an isolated airfoil is $V_f^* = 5.47$. The flutter speed for model 1 is $V_f^* = 6.6$, which is a 20% increase over that of an isolated airfoil. For this symmetric configuration, the wing acts like an obstacle in the stream that slows down the flow approaching the tail. Consequently, the shock on the tail is moved upstream and decreased in strength. The flutter speed is hence increased (a favorable effect). The flutter speed for model 2 is $V_f^* = 4.7$, which is a 14% decrease over that of an isolated NACA 0012. For this asymmetrical case, the negative lift on the wing produces an upwash that increases the effective angle of attack of the tail. This counteracts the obstacle effect of the wing, and the net result is a decrease in the flutter speed (an unfavorable effect). Note that if the tail itself has a nonzero angle of attack, the effect of the upwash generated by the wing can be either favorable or unfavorable, depending on whether the tail effective angle of attack is increased or decreased. It is unfavorable if increased, favorable otherwise. An interesting and important problem is then, what would happen if the wing is oscillating and an oscillating wake is generated?

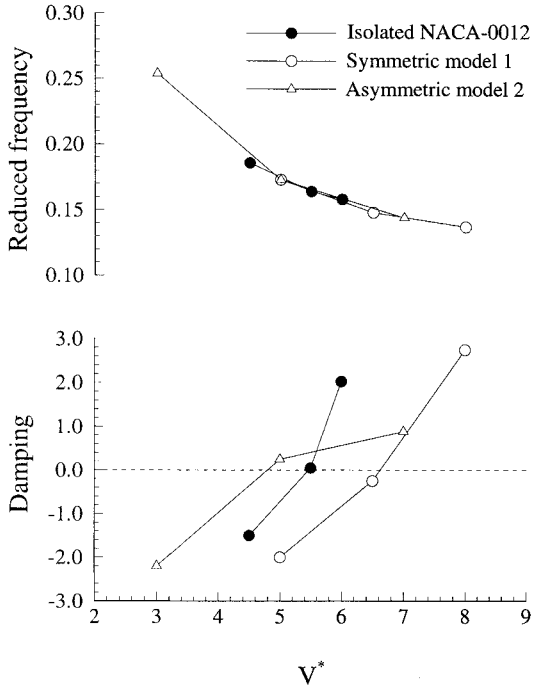


**Fig. 1 Modal damping and reduced frequency measured from the plunging displacement curves for an isolated NACA 0012, model 1 and model 2 configuration with a stationary forewing.**

## Tail Flutter with an Oscillating Forewing

The symmetric model 1 is used to investigate the tail flutter under the influence of an oscillating forewing. The wing is forced to pitch about its quarter-chord point following $\alpha = 3° \sin(2M_\infty \kappa_w t)$ where the wing reduced frequency is $\kappa_w = 0.2$. The freestream has $M_\infty = 0.8$ and zero angle of attack. The structural parameters are the same as given by Isogai.[10] The steady-state solution with a stationary wing is obtained first and employed as the initial condition. The wing starts to pitch at $t = 0$, and at the same instant the tail is released to move according to output of the aeroelastic solver. The Euler implicit method is used to integrate the flow solver, and about 3000 time steps are taken to complete one cycle of wing oscillation.

Figure 2 shows the plunging and the pitching displacement curves and their FFT spectra for various $V^*$. Note that the two displacements are in phase with different amplitudes. This is the result of the chosen structural parameters. In general, two frequencies can be identified in the FFT spectra. One is the prescribed frequency of the wing oscillation that represents the external forcing to the tail aeroelastic system. The corresponding tail response to this external forcing is a forced oscillation at the prescribed "forcing" frequency $f_f$. The other is the "characteristic" frequency $f_c$ of the tail aeroelastic system when subjected to some disturbances. The corresponding tail motion is a transient response at the characteristic frequency of the system. This transient response may eventually die out or grow pending on the nonlinear interactions among the aerodynamic and the structural conditions of the system. In fact, the characteristic frequency is the flutter frequency when the system flutters.

Figure 2a shows the computed results for $V^* = 3$. It is seen that the two modes of tail motion combine to exhibit the "beat" pattern for $t < 200$, but eventually the transient mode diminishes and only the forced mode persists to become a limit cycle oscillation with finite amplitude. Figure 2b shows the data set for $V^* = 4$. Only one peak at the forcing frequency is identified in the FFT spectra, which indicates the condition of resonance. The tail displacements grow rapidly with time initially and soon become an order of magnitude greater than those for $V^* \leq 3.5$. Figure 2c shows the data set for $V^* = 5$. The behaviors of the tail motion are basically the same as those for $V^* \leq 3.5$. But here the transient mode lasts longer and the beat pattern is more profound. Figure 2d shows the data set for $V^* = 6$. The envelope of the displacement curves is almost constant. This implies that $V^* = 6$ is close to the neutral stability boundary at which the transient mode of the tail motion neither grows nor dies. The two modes of the tail motion show equal strength in the FFT spectra. Figure 2e shows the data set for $V^* = 7$. The envelopes of the displacement curve grow rapidly with increasing rate, indicating an unstable situation. The dominate peak in the FFT spectra is at the characteristic frequency, indicating that it is the transient mode that is unstable.

Judging from Fig. 2, it is seen that displacement curves behave differently for different $V^*$ values. It shows a damped oscillation for $V^* \leq 3.5$, a monotone increase for $V^* = 4$, a damped oscillation again for $4.5 \leq V^* \leq 5$, a neutral oscillation for $V^* = 6$, and finally an excited oscillation for $V^* \geq 6.5$. The data indicate that for $V^* \leq 6$ with a possible exception of $V^* = 4$, the tail will eventually enter into a limit cycle

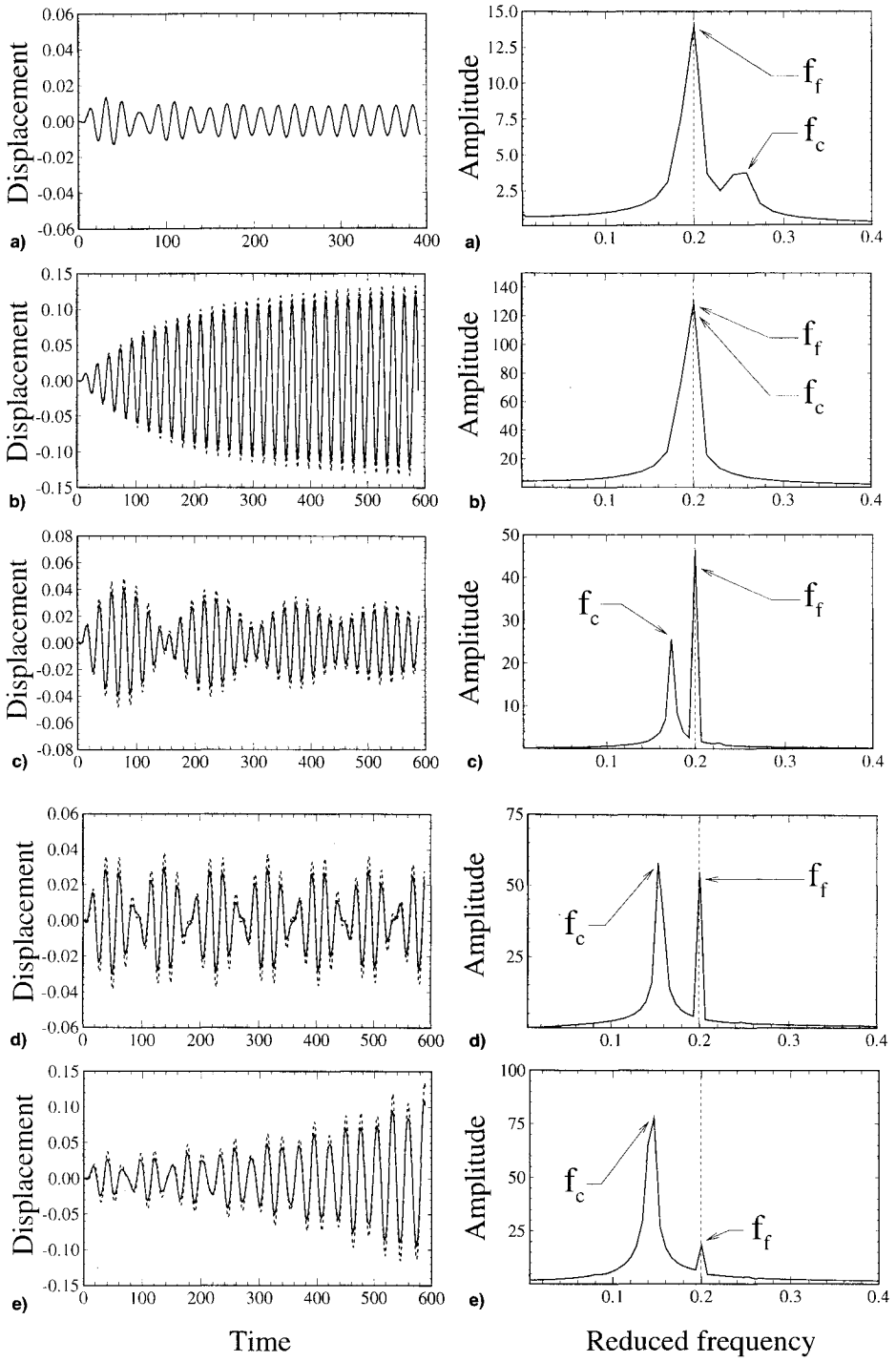


**Fig. 2 Tail flutter analyses with an oscillating forewing for the symmetric model 1, left column: plunging (line) and pitching (dashes) displacement curves, right column: FFT frequency spectra of plunging displacement, $f_f$ and $f_c$, $V^*$ = a) 3, b) 4, c) 5, d) 6, and e) 7.**

oscillation with finite amplitude at the forcing frequency. For $V^* = 4$, resonance occurs between the forcing frequency and the characteristic frequency, and the amplitude of the oscillation is a maximum. For $V^* > 6$, the transient mode continues to grow within the recorded time with increasing rate. It is reasonable to suggest that, similar to the flutter boundary, there is a stability boundary around $V^* = 6$, above which the transient mode of the tail response will be excited. Recall that the tail flutter boundary is $V^* = 6.6$ with a stationary forewing. This is a 9% drop in flutter boundary due to the wing oscillation.

Figure 3 shows the computed peak height of plunging displacement at the end of each computation for different $V^*$. Note that while most of the computations terminate at $t = 600$, some cases terminate when a stable finite amplitude oscillation is resulted. Within the recorded time, there is a local maximum in the computed displacement at $V^* = 4$. This is the characteristics of resonance. After $V^* > 6$, the computed displacement increases rapidly with increasing $V^*$. This is the characteristics of flutter. In this study, resonance is worthy of our attention because it occurs before the onset of flutter. For the given flow conditions and structural parameters, Fig. 4 shows the variation of characteristic frequency with $V^*$. Figure 4 is the curve on which the resonance occurs. For example, resonance condition similar to Fig. 2b is obtained with a wing pitching at $\kappa_w = 0.369$ and $V^* = 2$.

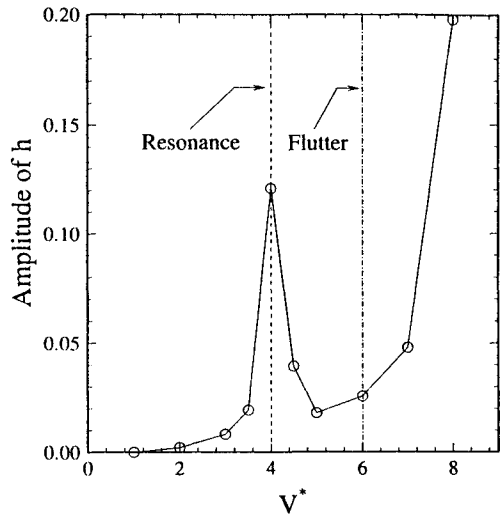


**Fig. 3 Tail flutter analyses with an oscillating forewing for the symmetric model 1, computed peak of the plunging displacement curve at the end of each computation for different $V^*$.**

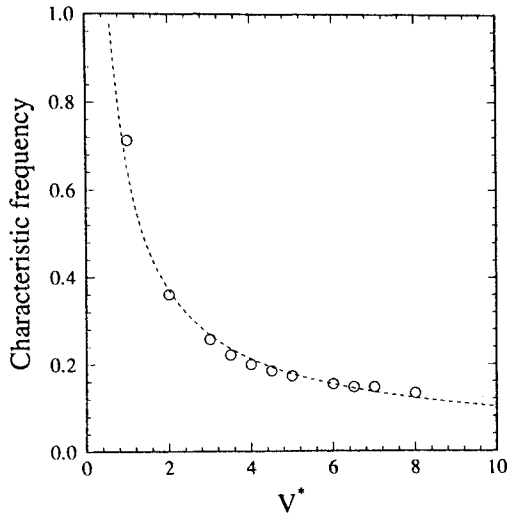


**Fig. 4 Tail flutter analyses with an oscillating forewing for the symmetric model 1, tail characteristic frequency $f_c$ at different $V^*$, symbols: computed, dashes: curve fit of computed data $f_c(V^*)^{0.803} = 0.648$.**

## Conclusions

An upwind Euler solver on unstructured dynamic mesh and a two-degree-of-freedom aeroelastic solver are coupled to examine the flutter boundary of two-dimensional wing–tail configurations. The effects of a stationary forewing on the tail flutter are twofold. First, the wing acts like an obstacle in airstream, which slows down the flow approaching the tail. The tail flutter boundary is hence increased (a favorable effect). Second, a downwash is generated on the tail that may be favorable if the effective angle of attack is decreased, or unfavorable if otherwise. For the symmetric wing–tail configuration studied, when the forewing is pitching sinusoidally, there are two unfavorable effects on the tail aeroelastic behaviors. The first is a possible drop in the flutter boundary due to the wing oscillation. The second is a possible resonance between the forcing frequency of the wing motion and the characteristic frequency of the tail aeroelastic system. This resonance may occur before the onset of tail flutter. Both resonance and flutter encourage large amplitude oscillations, hence, they are dangerous to the tail structure.

## Acknowledgments

This work is partially supported by National Science Council under Contract NSC84-2212-E006-002. The authors thank P. J. Lu and D. Y. Yeh of IAA/NCKU for their contribution in the development of the aeroelastic solver.

## References

[1]Shankar, V., and Malmuth, N. D., "Transonic Flow Calculations over Two-Dimensional Canard-Wing Systems," *Journal of Aircraft*, Vol. 18, No. 2, 1981, pp. 108–114.

[2]Batina, J. T., "Unsteady Transonic Flow Calculations for Two-Dimensional Canard-Wing Configurations," *Journal of Aircraft*, Vol. 23, No. 4, 1986, pp. 190–198.

[3]Rausch, R. D., Batina, J. T., and Yang, T. Y., "Euler Flutter Analysis of Airfoils Using Unstructured Dynamic Meshes," *Journal of Aircraft*, Vol. 27, No. 5, 1990, pp. 436–443.

[4]Batina, J. T., "Unsteady Euler Algorithm with Unstructured Dynamic Meshes for Complex Aircraft Aerodynamic Analysis," *AIAA Journal*, Vol. 29, No. 3, 1991, pp. 327–333.

[5]Pan, D., and Cheng, J. C., "A Second-Order Upwind Finite-Volume Method for the Euler Solution on Unstructured Triangular Meshes," *International Journal for Numerical Methods in Fluids*, Vol. 16, No. 12, 1993, pp. 1079–1098.

[6]Pan, D., and Cheng, J. C., "Upwind Finite-Volume Navier-Stokes Computations on Unstructured Triangular Meshes," *AIAA Journal*, Vol. 31, No. 9, 1993, pp. 1618–1625.

[7]Vinokur, M., "Review Article: An Analysis of Finite-Difference and Finite-Volume Formulations of Conservation Laws," *Journal of Computational Physics*, Vol. 81, 1989, pp. 1–52.

[8]Edwards, J. W., Bennett, R. M., Whitlow, W., Jr., and Seidel, D. A., "Time-Marching Transonic Flutter Solutions Including Angle-of-Attack Effects," *Journal of Aircraft*, Vol. 20, No. 11, 1983, pp. 899–906.

[9]Bennert, R. M., and Desmarais, R. N., "Curve Fitting of Aeroelastic Transient Response Data with Exponential Functions," *Flutter Testing Techniques*, NASA SP-415, May 1975, pp. 53–58.

[10]Isogai, K., "Numerical Study of Transonic Flutter of a Two-Dimensional Airfoil," National Aerospace Lab., TR-617T, Tokyo, Japan, July 1980.

# Preconditioned Generalized Minimum Residual Acceleration of Panel Methods

Santhosh P. Koruthu*
*Aeronautical Development Agency, Bangalore 560017, India*

## Introduction

PANEL methods are among the most efficient methods for solving linearized potential flow problems. Therefore, these methods are used extensively in the design tradeoff studies for aircraft configurations.[1,2] The efficiency of these methods depends, to a large extent, on the method employed in solving the linear algebraic equations that arise in the discretized formulation. Iterative solvers are preferred over direct solvers, if convergence is guaranteed to be sufficiently fast. However, convergence may be very slow when using standard iterative solvers. Therefore, many panel codes use direct solvers.[3,4] Direct solutions can become very expensive if the number of panels is large such as when analyzing the flow past very complex aircraft configurations, where a large number of panels is required. Thus, there is a need to evaluate the applicability of new algorithms based on recent devel-

Received Jan. 17, 1995; revision received March 10, 1995; accepted for publication March 27, 1995. 

*Project Manager, P.B. No. 1718, Vimanapura Post.